Magmatic lulls in the Sierra Nevada captured in zircon from rhyolite of the Mineral King pendant, California

Erik W. Klemetti[1,*], Jade Star Lackey[2], and Jesslyn Starnes[1,3]
[1]*Department of Geosciences, Denison University, Granville, Ohio 43023, USA*
[2]*Geology Department, Pomona College, Claremont, California 91711, USA*
[3]*Earth and Planetary Sciences Department, University of California–Davis, Davis, California 95616, USA*

ABSTRACT

The Mineral King pendant in the Sierra Nevada batholith (California, USA) contains at least four rhyolite units that record high-silica volcanism during magmatic lulls in the Sierran magmatic arc. U-Th-Pb, trace element (single crystal spot analyses via sensitive high-resolution ion microprobe–reverse geometry, SHRIMP-RG), and bulk oxygen isotope analyses of zircon from these units provide a record of the age and compositional properties of the magmas that is not available from whole-rock analysis because of intense hydrothermal alteration of the pendant. U-Pb spot ages reveal that the Mineral King rhyolites are from two periods, the Early Jurassic (197 Ma) and the Early Cretaceous (134–136 Ma). These two rhyolite packages have zircons with distinct compositional trends for trace elements and $\delta^{18}O$; the Early Jurassic rhyolite shows less evidence of crustal influences on the rhyolites and the Early Cretaceous rhyolite shows evidence of increasing crustal influences and crystal recycling. These rhyolites capture evidence of magmatism during two periods of low magmatic flux in the Sierran Arc; however, they still show that magmas were derived from interactions of maturing continental crust, increasing from the Early to Late Jurassic. This finding likely reflects the transition of the North America margin from one of docking island arcs in the Early Jurassic to one of a more mature continental arc in the Early Cretaceous. This also shows the utility in examining zircon spot ages combined with trace element and bulk isotopic composition to unlock the petrogenetic history of altered volcanic rocks.

*Email: klemettie@denison.edu

INTRODUCTION

Whereas studies of Mesozoic magmatism in the Sierra Nevada arc (California, USA) are biased toward studies of voluminous plutonic units (e.g., Bateman, 1992; Chen and Moore, 1982; Glazner et al., 2004, Lackey et al., 2008; and many others), Triassic, Jurassic, and Cretaceous volcanic pendants and septa within the Sierra Nevada batholith commonly contain metamorphosed volcanic rocks that either predate or are coeval with the plutonic rocks that bound them (e.g., Kistler and Swanson, 1981; Busby-Spera, 1983; Saleeby et al., 1990; Fiske and Tobisch, 1994; Schweickert and Lahren, 1999; Barth et al., 2012). This includes notable volcanic packages at Erskine Canyon, in the southern Sierra Nevada, in the Oak Creek, Boyden Cave, and Goddard pendants in the Kings Canyon region, and in neighboring areas of the Alabama Hills and Inyo Range; a group of pendants with abundant metavolcanic rocks is found between Yosemite National Park and the Long Valley caldera. Although it is well known that metavolcanic rocks in pendants around Kings Canyon and to the north overlap in age and in some cases may be correlative, the Mineral King pendant in the south-central Sierra Nevada represents a key domain between shallower and deeper levels of the batholith, as well as major intrabatholithic structural breaks (Saleeby et al., 1978; Saleeby and Busby, 1993).

These metavolcanic remnants are a sparse but important record of magmatism in high levels of the Sierran Arc. However, interpretation of the history of these volcanic units is problematic because they are extensively deformed, hydrothermally altered, and contact metamorphosed (Hanson et al., 1993; Sorensen et al., 1998). Zircon contained within such volcanic rocks affords the clearest window into original magmatic conditions because its refractory nature (Harley and Kelly, 2007) makes it unaffected by the myriad effects of secondary alteration. In particular, U-Pb age data and isotopic and trace element information from zircon provide fresh insight into volcanism, as exemplified by studies of zircon from Triassic volcanic rocks in the Saddlebag Lake pendant (Lackey et al., 2008; Dietterich et al., 2009; Barth et al., 2012).

Aggregate plutonic and volcanic ages (Irwin and Wooden, 1999, 2001) show that rates of magmatism across the arc were not constant over its 150 m.y. life span, and prominent lulls in activity have been noted (Paterson, 2012; Barth et al., 2013). Little is known about these periods of quiescence due to their paucity within the geologic record. Any remnants from these periods of low magmatic activity contain information that is lost across much of the arc and begs the question of how magmatism was changing from the Late Triassic arc (Barth et al., 2012, 2013) to the Cretaceous batholith emplacement (e.g., Ducea, 2001; Glazner et al., 2004). Two end-member models could exist: (1) magmatism was very infrequent during these lulls, so mature magmatism systems would be rare, or (2) much of the magmatic record of magmatism has been lost (to erosion or burial) and mature magmatic system that exhibit abundant crystal recycling and rhyolite volcanism are active across the arc during the lulls. By assessing these patterns of magmatism across the history of the western North American margin, a better understanding of tempos of magmatism can accompany tectonic models for the evolution of the margin (Paterson, 2012).

In this study we present new zircon age and compositional data on four metavolcanic units from the Mineral King pendant in the central Sierra Nevada. These four units provide information about volcanic and intrusive activity on the western margin of North America during the Early Jurassic and Early Cretaceous. These units are rhyolite deposits related to arc magmatism, and the zircons from these rhyolites reveal the changing parameters of magmatism from ca.

Geosphere; February 2014; v. 10; no. 1; p. 66–79; doi:10.1130/GES00920.1; 11 figures; 2 tables; 6 supplemental files.
Received 26 February 2013 ♦ Revision received 1 November 2013 ♦ Accepted 14 November 2013 ♦ Published online 19 December 2013

197 Ma to ca. 134 Ma, suggesting an increase in the influence of continental crust and recycling of magmatic precursors. The zircons also imply that even during periods of low overall magmatic productivity in the western North American margin, voluminous rhyolite volcanism was occurring, with all the hallmarks of long-lived magmatic systems where magma is extracted from a crystal mush, promoting abundant crystal recycling. The data also show how the petrogenesis of altered volcanic rocks can be determined by the combination of single zircon spot ages and trace element analyses combined with bulk zircon oxygen isotopic analyses. This provides the opportunity to examine the important parameters of petrogenesis (fractional crystallization, assimilation, and mixing; e.g., see Claiborne et al., 2010a; Walker et al., 2010; Barth et al., 2012) on suites of silicic, zircon-bearing rocks that have hitherto been considered too altered to be assessed by whole-rock methods.

SETTING

The Mineral King pendant is located in the central Sierra Nevada in California (Fig. 1) and is one of the many septa and screens representing the wall rock into which the Sierra Nevada batholith intruded. The Mineral King pendant is constructed from metaigneous volcanic (rhyolite to andesite) and intrusive (gabbro and granite) units, breccia sandstones, marbles, and marine sediment (Busby-Spera, 1983; Saleeby and Busby, 1993; Sisson and Moore, 2013). Many of these units were altered by the intrusion of fluids and shearing (Bateman, 1992; D'Errico et al., 2012). These units are bound within the pendant by multiple faults and shear zones (Busby-Spera, 1983). The package of rock was interpreted as a marine sequence from the paleocontinental shelf of western North America (Busby-Spera and Saleeby, 1987; Saleeby and Busby, 1993), possibly representing 70 m.y. of continuous stratigraphy (Busby-Spera, 1983). The Mineral King pendant is bound to the east by the quartz diorite of Empire Mountain (ca. 109 Ma; D'Errico et al., 2012) and the granite of Coyote Pass (97 ± 2 Ma; Busby-Spera and Saleeby, 1987) and to the west by the granodiorite of Castle Creek (98 ± 2 Ma; Busby-Spera and Saleeby, 1987). Emplacement barometry of the eastern contact with the Empire quartz monzodiorite suggests shallow depths of <3 km (D'Errico et al., 2012). Overall, the Mineral King pendant has been broadly correlated with other pendants in the King Series (Saleeby and Busby, 1993).

There are four rhyolite units (R_0, R_1, R_2, R_4; Fig. 1) within the Mineral King pendant that have been interpreted as tuffs and flows from a submarine (or proximal) caldera (Busby-Spera, 1984, 1986). In total, ~90 km^3 of rhyolite tuffs have been documented in the Mineral King pendant, each ~20–25 km^3 in volume, along with 10 km^3 of andesite lavas and volcaniclastic units (Busby-Spera, 1984). These units were originally dated by Busby-Spera (1983) using multigrain zircon dissolution analyses combined with stratigraphic interpretation of the pendant. The R_0, R_1 and R_3 rhyolites were thought to be Early Triassic (215 ± 2 Ma). The R_4 (189 ± 2 Ma) and the R_2 were assigned to the Early Jurassic, the sediment in the pendant marking quiescence between eruptions (Busby-Spera, 1983). A volumetrically minor dacite intrusive breccia on the easternmost contact was dated as 240 ± 7 Ma (Busby-Spera, 1983). Structurally, the Empire fault separates the R_2 and R_4 units and the Farewell fault separates the R_0 and R_1 units from the R_2 and R_4 units (Fig. 1). Busby-Spera (1983) interpreted that the volcanism in the Mineral King pendant as the transition from an Early Triassic island arc (R_0, R_{01}, R_3, R_4 units) to an Early Jurassic continental arc (R_2 unit) as a continuous depositional sequence.

SAMPLE DESCRIPTIONS

The R_0 rhyolite (10JS03) is intruded by the Castle Creek granodiorite to the west, and the contact between the two units is indistinct and interfingering (Fig. 1). This unit is considerably altered to quartz sericite schist; few plagioclase feldspar phenocrysts remain. However, primary bedding of ashy and/or sandy layers are evident (Fig. 2A). Large (>1 cm to tens of centimeters) quartz veins with boudinage textures are present in outcrops near the contact with the Castle Creek. This unit has an estimated modal abundance of 55% quartz, 35%–45% mica (mostly biotite, some muscovite), and 5%–10% plagioclase feldspar.

The R_1 rhyolite (11MK02) is near the southwestern boundary of the pendant. It is bound to the west by a sandstone breccia, calc-silicate sediment, and an undated aplitic intrusion, and to the east by a slate unit that extends along the valley bottom (Fig. 1). As with all samples within the pendant, it has been altered to quartz sericite schist but retains relic textural fabrics of a rhyolite tuff (e.g., ghost-like pumice clasts; Fig. 2B). This unit has a modal abundance similar to that of R_0.

The R_2 rhyolite has no visible contacts with surrounding units and is bound to the east by calc-silicates and to the west by slate (Fig. 1). It is heavily altered, with relict phenocrysts visible on the weathered surfaces but not visible on fresh surfaces (Fig. 2C). There is abundant mica, and from west to east the outcrop grades from a rhyolite tuff to a flow-banded rhyolite. The unit has been altered to quartz sericite schist. Both biotite and muscovite micas are aligned in a clear foliation direction, particularly in the flow-banded portion of the unit. This unit has a modal abundance similar to that of R_0, but with a higher proportion of plagioclase feldspar versus micas.

The R_4 rhyolite is the least visibly altered of all the units, but is still classified as a quartz sericite schist. It is bound to the east by the Empire quartz monzodiorite (109 Ma; D'Errico et al., 2012) and to the west by the R_2 rhyolite, although the direct contact is not observed (Fig. 1). The outcrop displays a platy weathering pattern, and fresh surfaces have visible phenocrysts (Fig. 2D). Alignment of mafic crystals produces a slight fabric. This unit has an estimated modal abundance of 55% quartz, 20% mica (mainly biotite), 20% plagioclase feldspar, and 5% amphibole.

METHODS

Samples of the four major rhyolite units (R_0, R_1, R_2, R_4) within the Mineral King pendant were collected during the summers of 2010 and 2011. Although all of the units are metamorphosed (likely through heating and fluid involvement to hornfels facies), care was taken to choose samples that were fresh and still showed primary volcanic textures. Approximately 3 kg of sample were crushed and zircons were extracted from all samples using standard mineral separation techniques (see Klemetti et al., 2011) at Pomona College and California State University Bakersfield. Zircon crystals larger than 57 µm were mounted in epoxy and polished at the Stanford University–U.S. Geological Survey Micro Analysis Center (SUMAC laboratory). Prior to SHRIMP-RG (sensitive high-resolution ion microprobe–reverse geometry) analysis, all samples were imaged via cathodoluminescence (CL) (Fig. 3) to assess the zoning and dissolution patterns along with melt and/or mineral inclusions within the grains. Analyses for U-Pb ages (Supplemental Table 1[1]) and trace elements (Supplemental Table 2[2]) in the zircons

[1]Supplemental Table 1. Full U-Pb isotopic data collected via SHRIMP-RG for zircon of the Mineral King pendant rhyolite units. All errors listed are 1σ. If you are viewing the PDF of this paper or reading it offline, please visit http://dx.doi.org/10.1130/GES00920.S1 or the full-text article on www.gsapubs.org to view Supplemental Table 1.

[2]Supplemental Table 2. Trace element data collected via SHRIMP-RG for zircon of the Mineral King pendant rhyolite units. Ages for samples are weighted mean ages with 1σ errors. Normalized elements are versus Bulk Silicate Earth of MacDonough and Sun (1995). If you are viewing the PDF of this paper or reading it offline, please visit http://dx.doi.org/10.1130/GES00920.S2 or the full-text article on www.gsapubs.org to view Supplemental Table 2.

were performed via SHRIMP-RG using methods from Mazdab and Wooden (2006) and all data were reduced using Isoplot 4 and SQUID2 software (http://www.bgc.org/isoplot_etc/squid.html) (Table 1; Supplemental Table 1 [see footnote 1]; Ludwig, 2003). We report $^{206}Pb/^{238}U$ ages corrected by measured values of ^{207}Pb (Supplemental Table 1 [see footnote 1]). Conventional concordia (Supplemental Figure[3]) and weighted mean age diagrams (Fig. 4) were constructed using Isoplot (Ludwig, 2003). Samples of the R33 zircon (419 Ma) standard were analyzed to correct for instrumental drift and reproducibility for U-Pb age determination and samples of the MAD in-house zircon were used for trace element reproducibility (Supplemental Table 2 [see footnote 2]). All errors on final ages are 1σ unless noted otherwise.

Because zircons in the Mineral King rhyolites show simple population traits by CL (i.e., no rim or core CL differences that suggest secondary ion mass spectrometry analysis is warranted; Fig. 3; Lackey et al., 2013), bulk laser fluorination oxygen isotope analysis was used to provide an accurate and precise measure of magmatic $\delta^{18}O$ (King et al., 1997). Oxygen isotopic analyses of bulk zircon separates were performed at the Stable Isotope Laboratory at the University of Oregon. Zircon concentrates were prepared for $\delta^{18}O$ analysis by sequentially cleaning bulk aliquots in HNO_3, HF, and HCl to remove mineral impurities and radiation-damaged domains from the crystals (Lackey et al., 2008). Oxygen was liberated from zircon by laser fluorination at the University of Oregon Stable Isotope Lab using a 35W New Wave CO_2 infrared laser to heat samples in the presence of BrF_5 reagent (Bindeman, 2008). Oxygen was cryogenically cleaned, pumped through hot Hg to capture excess F_2, and converted to CO_2 with a hot carbon rod before analysis. Isotope ratios were measured with a Finnigan MAT 253 mass spectrometer and measured values were corrected to the Gore Mountain garnet standard (UWG-2) analyzed throughout the session using the accepted $\delta^{18}O$ value of 5.80‰ (Valley et al., 1995). The average raw $\delta^{18}O$ of UWG-2 for 2 days of analyses (n = 6) in this study is 5.75‰ ± 0.12‰ (2σ).

We measured major and selected trace elements for three samples by X-ray fluorescence (Supplemental Table 3[4]) at Pomona College. Rock powder and flux were vortex blended in a 1:2 ratio (3.5 g powder to 7.0 g dilithium tetraborate), and fused to glass beads in graphite crucibles heated at 1000 °C for 10 min. Beads were reground and fused a second time, polished on diamond laps, and analyzed. Concentrations were determined according to calibrations based on 55 certified reference materials that span a large range of compositions (see Lackey et al., 2012, for further details regarding X-ray fluorescence analysis at Pomona College). Typical analytical 2σ uncertainties for analyses (in wt%) of major elements, determined conservatively as reproducibility of multiple beads produced from a sample or standard powder, are ±0.15% SiO_2; 0.06%–0.07% Fe_2O_3, Al_2O_3; 0.02%–0.05% Na_2O, K_2O, MgO, CaO; <0.004% TiO_2, MnO, P_2O_5. Trace element uncertainties at ppm ± 2σ are 1 ppm La, Pr, Hf; 2 ppm Nd, Cu, Ga, Nb, Pb, Rb, Th, U, Y, Zr; to 3 ppm Cr, Sc, Sr, V; other elements have higher uncertainties: Ce 4 ppm; Zn 6 ppm; Ni 7 ppm; Ba 30 ppm.

DATA

Zircon CL Zoning

CL images of zircons from the Mineral King metavolcanic rhyolite units show that most of the crystals have not undergone much if any alteration since their primary igneous formation (Fig. 3). The zircon samples are typically a few hundred micrometers in length. The crystals are variably cored, some with dark, U-rich cores that exhibit minor dissolution (rounded shapes relative to the euhedral outer zoning) with regular, oscillatory zoning with euhedral crystal shapes (Fig. 3). Some other cores observed have mottled cores with abundant melt inclusions and light colored cores that lack any evidence of zoning. There is no noticeable difference in the shapes and sizes of zircons or in zonation between zircons from any of the rhyolite units.

Zircon U-Pb Spot Ages

We performed 51 spot analyses on zircons culled from the 4 Mineral King metavolcanic units. Table 1 summarizes the age information determined from the ^{238}U-^{206}Pb analyses and Supplemental Table 1 (see footnote 1) contains the full complement of U-Pb analysis data. In all, three units (R_0, R_1, R_2) yielded weighted mean ages of 136.5 ± 2.7, 134.2 ± 0.7, and 135.5 ± 1.4 Ma, respectively, and one unit (R_4) yielded an age of 195.7 ± 1.4 Ma (1σ errors; Fig. 4; Table 1). We have chosen weighted mean ages for the geochronology in this study as it encapsulates the complex nature of zircon populations in igneous rocks by examining the range of ages, looking for the highest density of ages for the chosen age. However, using the youngest ages derived from zircons that did not exhibit Pb loss as an eruption age does not significantly change the age interpretation of the units (Fig. 4; Table 1). Most samples had at least one grain that showed potential Pb loss with ages younger than the overall population, and these grains were rejected when calculating the weighed mean ages unless noted. Two zircons analyzed on the R_0 rhyolite had younger ages (128.9 ± 1.2 Ma and 129.5 ± 0.9 Ma, 1σ error) that caused a higher MSWD (mean square of weighted deviate; 12) for the weighted mean age (Fig. 4). However, the exclusion of these zircons does not affect the age determination significantly, although it reduces the MSWD. If the youngest 2 grains are excluded, the weighted mean age is 137.6 ± 2.0 Ma (MSWD 5.2) and if an additional 2 oldest ages are excluded, the weighted mean age becomes 135.5 ± 1.1 Ma (MSWD 0.86). We choose to retain all the zircon from this sample in the calculation of the weighted mean age even though it does not produce the lowest MSWD, as all calculated ages are within error. The R_0 rhyolite also yielded a single xenocrystic zircon with an age of 1.63 Ga ± 8.4 Ma (1σ; Table 1).

Zircon Trace Element Compositions

Trace element analyses (n = 65) from Mineral King zircons were performed (some of which do not have corresponding U-Pb analyses), a compilation of which is in Supplemental Table 2 (see footnote 2). The Mineral King rhyolite units show the general patterns seen in zircon, with enriched heavy rare earth element (HREE) versus light REE (bulk silicate Earth normalized; Sano et al., 2002), positive Ce anomalies, and modest Eu anomalies (Fig. 5). Two zircon analyses (10JS03–3.1, 10JS04–2.1) show enrichment across all trace elements (Fig. 5; Supplemental Table 2 [see footnote 2]); this may reflect growth in more fractionated liquid or small inclusions within the zircon that did not affect all trace elements analyzed. Zircons with anomalous values (such as high values of K, Ca, or Fe) were rejected from this compilation because they probably included analyses of mineral or glass inclusions (Supplemental Table 2 [see footnote 2]).

[3]Supplemental Figure. Conventional concordia diagrams for zircon of the Mineral King pendant rhyolite units. Conventional concordia diagrams ($^{207}Pb/^{235}U$ versus $^{206}Pb/^{238}U$) constructed using Isoplot 3.0 (Ludwig, 2003). Error ellipses are 2σ. Error on age derived from concordia diagram is 1σ. All samples produce an age that is within error of the weighted mean age, except for R_0, which does not produce a concordant age when all sample points are included. If you are viewing the PDF of this paper or reading it offline, please visit http://dx.doi.org/10.1130/GES00920.S3 or the full-text article on www.gsapubs.org to view the Supplemental Figure.

[4]Supplemental Table 3. X-ray fluorescence major and trace element analyses for whole-rock samples of the Mineral King pendant rhyolites. If you are viewing the PDF of this paper or reading it offline, please visit http://dx.doi.org/10.1130/GES00920.S4 or the full-text article on www.gsapubs.org to view Supplemental Table 3.

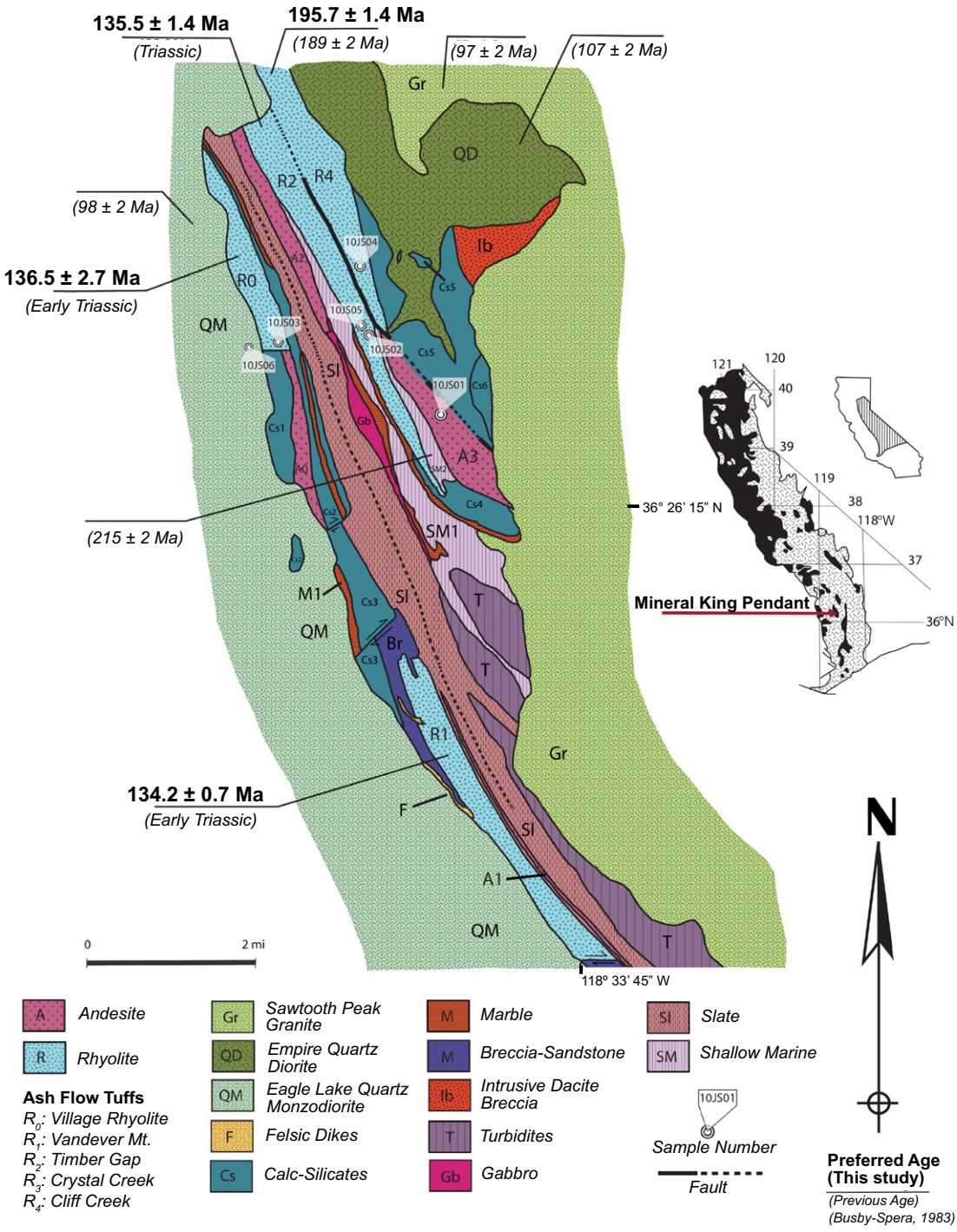

Figure 1. Geologic map of the Mineral King pendant (California, USA). Schematic map of the important units in the Mineral King pendant is modified from Busby-Spera and Saleeby (1987). Ages listed in bold are from this study. Ages in italics are from Busby-Spera (1983). All age errors are 1σ.

Zircons from the Mineral King rhyolite units range in Hf concentration from 7525 to 12800 ppm (Fig. 6). Overall, the R_0 and R_1 rhyolites have the widest range in Hf concentrations (8088–12800 ppm), the R_2 rhyolites has the lowest average Hf concentration (7525–10280 ppm), and the R_4 rhyolites is the most restricted (9081–10270 ppm; Fig. 6). These patterns are reflected across most trace element patterns. The R_0 and R_1 rhyolites represent the wider range of values, while the R_2 and R_4 rhyolites are more restricted, although many times the patterns overlap (Fig. 6). The U concentrations vary from 511 to 5127 ppm, and Th concentrations vary from 47 to 2618 ppm (Fig. 6), producing a range of Th/U of 0.114–1.449 (Fig. 7).

Zircons show a wide range of Eu/Eu*, from 0.11 to 0.49 (Figs. 6 and 7). The R_0 and R_1 zir-

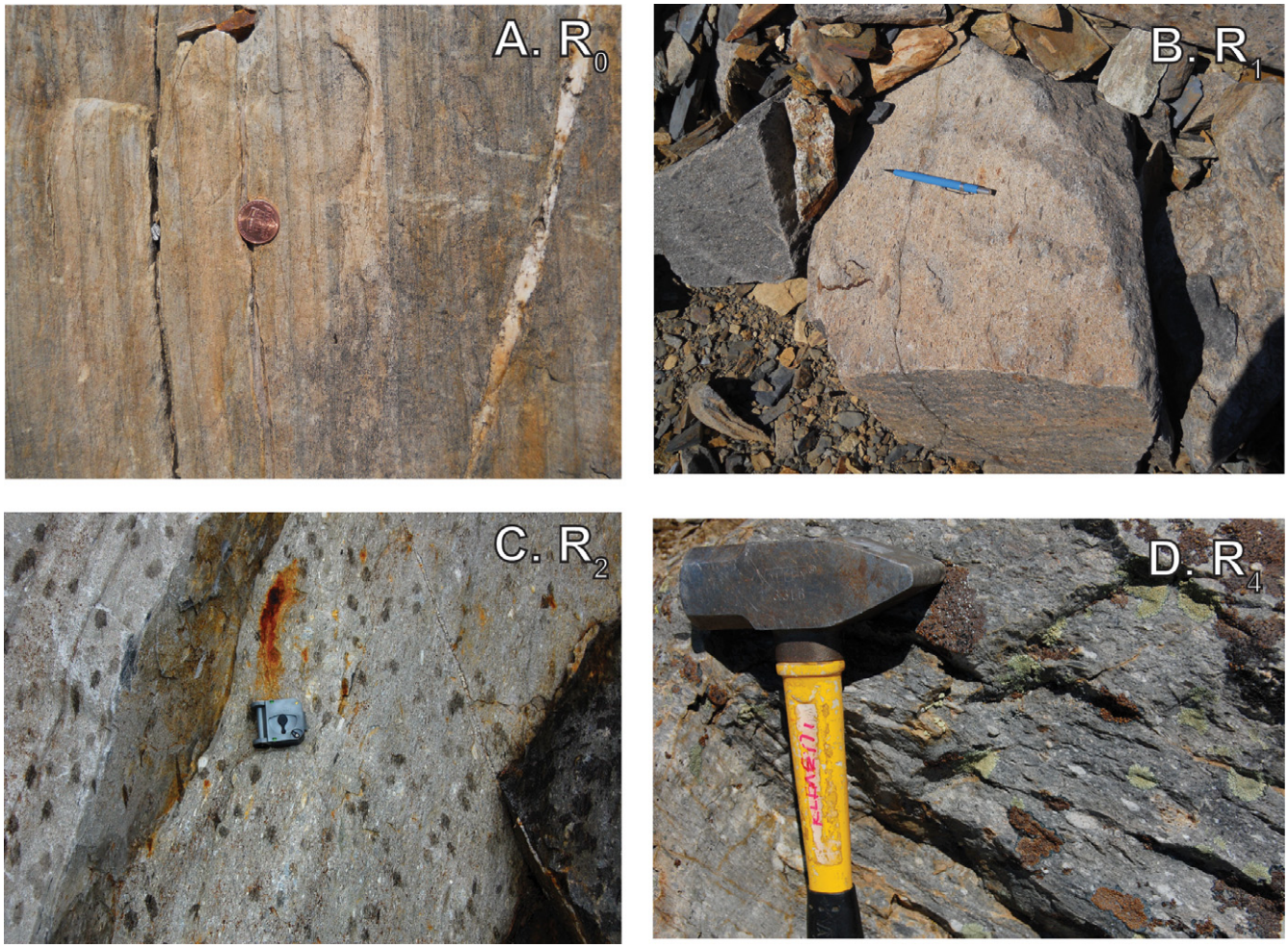

Figure 2. Outcrop photographs of the Mineral King rhyolite units sampled in this study. (A) The R_0 rhyolite, near the Mineral King road east of the National Park Service ranger station (coin is 19 mm diameter). (B) The R_1 rhyolite on the southeastern slope of Vandever Mountain. (C) The R_2 rhyolite, along the trail toward Monarch Lakes. (D) The R_4 rhyolite, along the western slopes of Empire Mountain. See text for descriptions of each sample.

cons show the greatest variability, spanning the entire range of Eu/Eu* in Mineral King rhyolite zircon. The R_2 zircons have a smaller range, only reaching Eu/Eu* of ~0.3, and the R_4 zircons have the most limited range, all between 0.22 and 0.26. The range in Yb/Gd ratios over all the units is 6.96–37.88 (Fig. 7), with similar patterns: the R_0 and R_1 rhyolites encompass the entire range, the R_2 rhyolite ranges from 10 to 20.3, and the R_4 rhyolite ranges from 14.1 to 26.7 (Fig. 7).

Zircon Oxygen Isotopic Compositions

Bulk zircon oxygen isotopic compositions of zircons provide an accurate and precise measure of overall magmatic $\delta^{18}O$ in altered volcanic rocks (cf. King et al., 1997). Three of the Mineral King rhyolite units yielded a range of $\delta^{18}O$ (zircon, Zrn) from 5.33‰ to 7.33‰ (Table 1). The oldest unit (R_4, 195.7 ± 1.4 Ma) had the lowest $\delta^{18}O$(Zrn) (5.33‰ ± 0.09‰), while the youngest units (R_0 and R_1, 136.5 ± 2.7 and 134.2 ± 0.7 Ma, respectively) had the highest $\delta^{18}O$(Zrn) (6.78‰ ± 0.08‰ and 7.33‰ ± 0.16‰, respectively). Fractionation of oxygen isotopes between zircon and magma, $\Delta^{18}O$(Zrn), can be calculated according to SiO_2 content of magma (Lackey et al., 2008; see Supplemental Table 3 [see footnote 4] for whole-rock analyses). Thus, magmatic $\Delta^{18}O$ values for the Mineral King metarhyolite units are 7.33‰ to 9.33‰.

DISCUSSION

Age of the Mineral King Metavolcanics

Previous studies (Busby-Spera, 1983; Saleeby and Busby, 1993) that examined the metavolcanic rocks of the Mineral King pendant used bulk zircon dissolution U-Pb geochronology and fossil correlation and/or stratigraphy to determine the relative age relationships of the units (Fig. 1). The conclusion was that the youngest rocks of the pendant were located on the east side in the R_4 rhyolite and the rhyolite units (and interbedded metasediments) became older to the west, with Triassic ages for the R_0 rhyolite (Busby-Spera, 1983). There were some complications to this order, because the intrusive dacite breccia on the far eastern side of the pendant was dated as 217 Ma (Busby-Spera and Saleeby, 1987), but overall, Busby-Spera (1983) interpreted the metavolcanic and metasedimentary rocks of the Mineral King pendant as a nearly continuous record of volcanic and sedimentary deposition from the Triassic to Early Jurassic.

Our findings indicate that the stratigraphy across the Mineral King pendant is much more complex (Fig. 1) than as concluded by Busby-Spera (1983). As the U-Pb analyses of single zir-

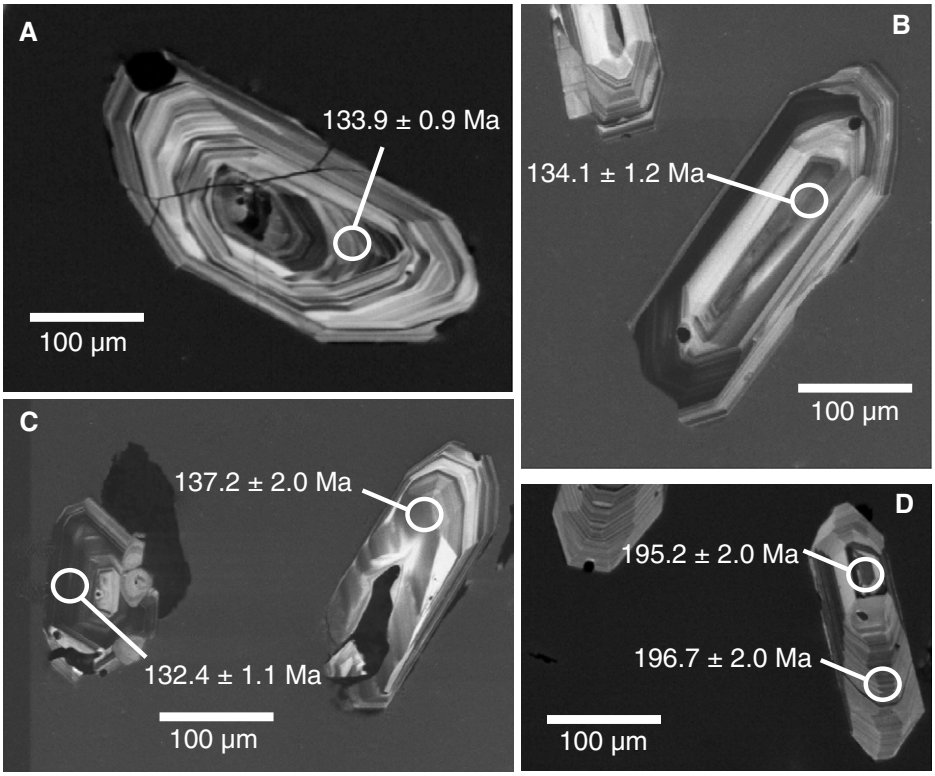

Figure 3. Cathodoluminescent images of selected zircon from rhyolites of the Mineral King pendant. White circle are spots for U-Pb and trace element analyses via SHRIMP-RG (sensitive high-resolution ion microprobe–reverse geometry), with ages. (A) 10JS03–7.1 from the R_0 rhyolite. (B) 11MK02–9.1 from the R_1 rhyolite. (C) 11MK02–7.1 and 11MK02–8.1 from the R_1 rhyolite. (D) 10JS04–3.1 and 10JS04–3.2 from the R_2 rhyolite. All errors are 1σ (see Supplemental Table 1 [see footnote 1]).

con grains from multiple igneous units across the pendant show (Fig. 4; Table 1), there is not a clear age progression from east to west across the pendant. When compared to ages from Busby-Spera (1983), starting from the east, the R_4 rhyolite is Early Jurassic in age, with a weighted mean age of 195.7 ± 1.4 Ma; this age is slightly older than the previous age of 189 ± 2 Ma. The R_2 rhyolite produced an age of 135.5 ± 1.4 Ma, significantly younger than the inferred Early Jurassic age. The R1 rhyolite produced a similar age of 134.2 ± 0.7 Ma rather than Early Triassic, while the R0 rhyolite yielded an age of 136.5 ± 2.7 Ma, compared to Early Triassic. Multiple samples from Busby-Spera (1983) were discordant and the presence of xenocrystic zircon with ages older than 1.6 Ga in the R_0 rhyolite would support the idea that the bulk zircon dissolutions were contaminated by these much older grains, thus skewing the data toward older, discordant ages.

Correlation of the Mineral King Metavolcanics

One important question to resolve when examining the metavolcanic units in the Mineral King pendant is whether they represent discrete events or a dismembered single volcanic package. Based solely on the geochronology, it is clear that the R_4 rhyolite is separated by more than 60 m.y. from the other dated rhyolite units within the pendant. However, the R_2, R_1, and R_0 units are within error of each other in age, so other factors must be considered in order to determine if they are separate rhyolite units (as suggested by Busby-Spera, 1983, 1984) or dismembered remains of a single rhyolite unit. One way to approach this issue is to look at the trace element compositions of the zircons found in the various metavolcanic units. Although the units are altered, the refractory nature of zircon allows for it to record magmatic conditions even if much of the rock host has been altered (Harley and Kelly, 2007). By comparing the compositional populations of zircon within each unit, it can be determined if R_2, R_1, and R_0 are likely to be the same rhyolite unit.

There are clear differences in the trace element compositions of zircons from the R_4 rhyolite and the R_0, R_1, and R_2 rhyolites (Figs. 4–8). The tight clustering of the zircons from the R_4 across multiple trace element parameters (Figs. 6 and 7) suggests that the rhyolite does not contain a large component of recycled zircon, either from the host rocks or from precursory silicic intrusions. This is supported by the lowest $\delta^{18}O$(Zrn) values in the Mineral King metarhyolites in the R_4 rhyolite (Table 1), precluding abundant assimilation of continental crust that tends to have higher values due to abundant quartz and feldspar (James et al., 1985). The R_4 rhyolite also has the lowest REE abundances of any metarhyolite unit within the Mineral King pendant (Fig. 5).

The R_0, R_1, and R_2 rhyolites are more complex, with a wider range of values across various trace element parameters (Figs. 6–8), suggesting an increased importance of zircon recycling within these youngest rhyolite units. The R_0, R_1, and R_2 rhyolite may share compositional and temporal attributes (Busby-Spera, 1983). However, our new data support the idea that these do not appear to be a single rhyolite unit sheared by the structures within the Mineral King pendant. By using the trace element compositions of zircons from these units, some broad observations can be made. First, the zircon from the R_2 rhyolite is compositionally distinct from zircon from the

TABLE 1. AGES AND COMPOSITIONS OF ZIRCON FROM METAIGNEOUS ROCKS IN THE MINERAL KING PENDANT

Sample	Unit	Previous age* (Ma)	New age† (Ma)	Error§ (Ma)	MSWD	Number of analyses	Minimum age (Ma)	Maximum age (Ma)	Xenocrysts?	$\delta^{18}O_{Zircon}$ (‰)
10JS03	R_0	Early Triassic	136.5	2.7	12	7	128.9	140.8	1.63 Ga**	6.78 ± 0.08
11MK02	R_1	Early Triassic	134.2	0.7	0.67	13	132.8	135.4	No	7.33 ± 0.16
10JS05	R_2	Triassic	135.5	1.4	2.6	9	132.4	137.8	No	n/a
10JS04	R_4	189 ± 2 Ma	195.7	1.4	1.2	13	191.6	199.5	No	5.33 ± 0.09

Note: MSWD—mean square of weighted deviates; n/a—none available.
*Previous ages from Busby-Spera (1983).
†Ages are weighted mean ages from ^{207}Pb-corrected $^{206}Pb/^{238}U$ analyzed via SHRIMP-RG (sensitive high-resolution ion microprobe–reverse geometry).
§All errors listed as 2σ. See Figure 1 for unit location and definition.
**Single zircon age.

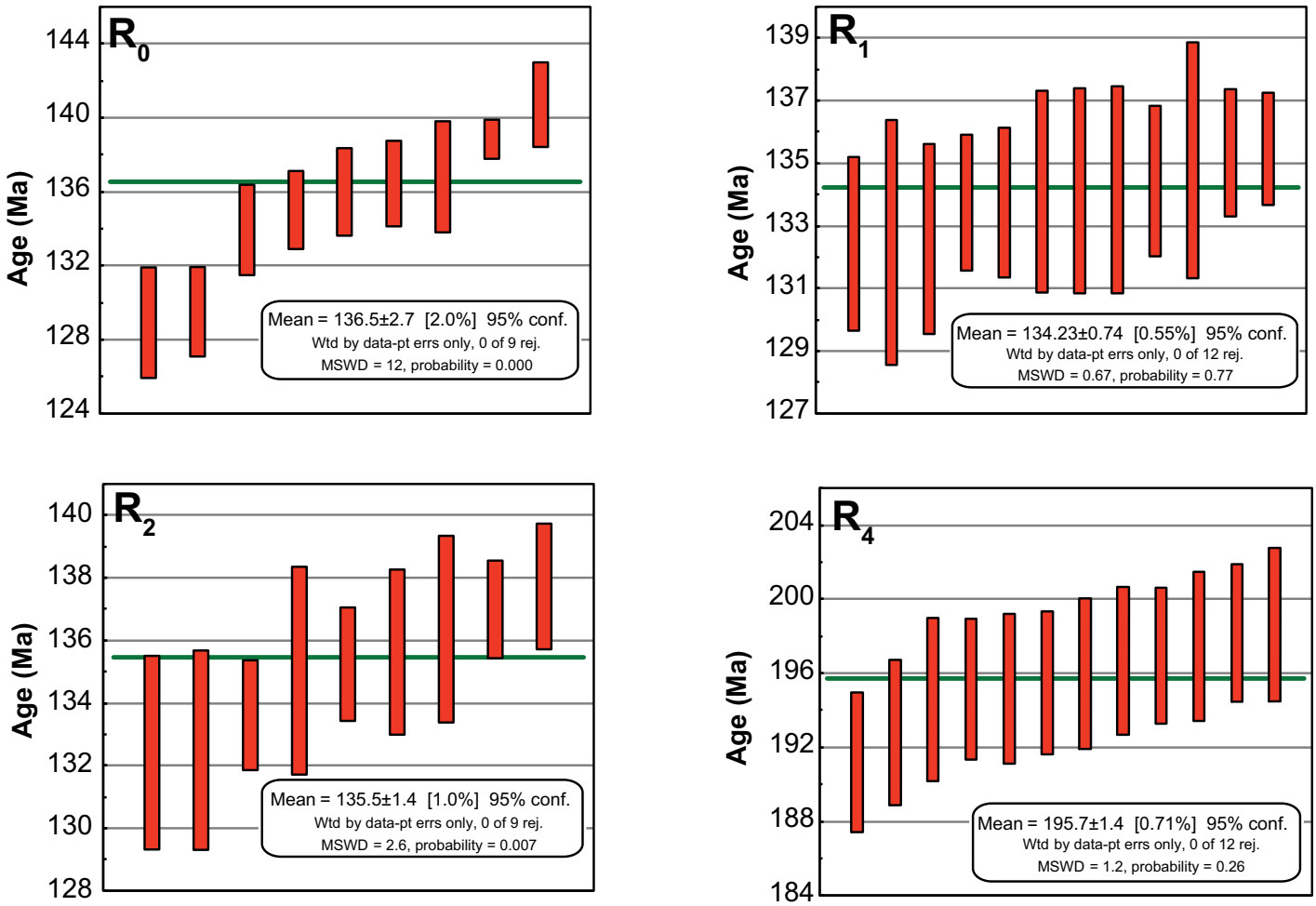

Figure 4. Weighted-mean age spectra for zircon analyses from the Mineral King pendant rhyolites. Ages listed are preferred ages based on the distribution of ages from zircon. The R_0 rhyolite had 2 zircons with ages outside of the error of the other 7 zircons. If these 2 zircons are not included in the age determination, the weighted mean age is 137.6 ± 2.0 Ma (mean square of weighted deviates, MSWD = 5.2). See Supplemental Table 1 (see footnote 1) for full U-Pb data and conventional concordia diagrams. All age errors are 1σ. Abbreviations: Wtd—weighted; pt—point; errs—errors; rej.—rejected; conf.—confidence.

R_0 and R_1 rhyolites. Although all three of these metarhyolites have ages within error of each other, the R_2 shows distinct zircon trace element compositions (Figs. 6 and 7): lower Hf concentrations along with higher Th/U, lower Yb/Gd, and higher Ce/Ce* at constant Hf concentrations. These trace element parameters suggest that the R_2 rhyolite was hotter (Miller et al., 2003), although the Eu/Eu* (Fig. 6) for the R_2 rhyolite is within the same range as the R_0 and R_1 rhyolites. The R_2 rhyolite also has overall higher REE concentrations versus the R_0 and R_1 rhyolites (Fig. 5).

The R_0 and R_1 rhyolites have a wider range in most trace element parameters relative to the R_2 rhyolite and have minor overlap with R_2 rhyolite compositions. These differences could mean that the R_2 rhyolite is the product of a different eruptive center that was brought into the Mineral King pendant via structural motion along a fault, or that the R_2 rhyolite is a compositionally earlier magma produced by the same eruptive center as the R_0 and R_1 rhyolites. Although the ages of these three units are within error, the presence of zircons with compositions similar to those of the R_2 in the R_0 and R_1 rhyolites suggests that they may have been derived from the R_2 residue. However, it is not possible, based on the evidence presented here, to conclusively differentiate between separate nearby eruptions or temporally separated eruptions from the same eruptive center.

Origins of the Mineral King Rhyolites

The rhyolites of the Mineral King pendant capture the magmatism within the western margin of North America during a period of relative magmatic quiescence (Barth et al., 2013; Figs. 9A, 9B). The zircon compositions of these rhyolite units allow a glimpse into the magmatic processes at work when these rhyolites formed and how those processes have changed over the 60 m.y. recorded in the pendant. Through the trace element and oxygen isotope composition of these zircons, three general observations can be made across the history of the Mineral King pendant (Fig. 1). (1) The zircon compositional populations change from tightly clustered in the 195.7 Ma R_4 rhyolite to more dispersed in the 134–136 Ma R_0, R_1, and R_2 rhyolites (Fig. 4). (2) The $\delta^{18}O$(Zrn) (Table 1) increases from the R_4 rhyolite (~5.33‰) to the R_0, R_1, and R_2 rhyolites (6.78‰–7.33‰). (3) The Th concentrations in zircons increase from <100 ppm in the R_4 rhyolite to >100 ppm in the R_0, R_1, and R_2 rhyolite (Fig. 6). All these parameters suggest an increased role in recycling and/or incorporation of continental material and/or silicic intrusive

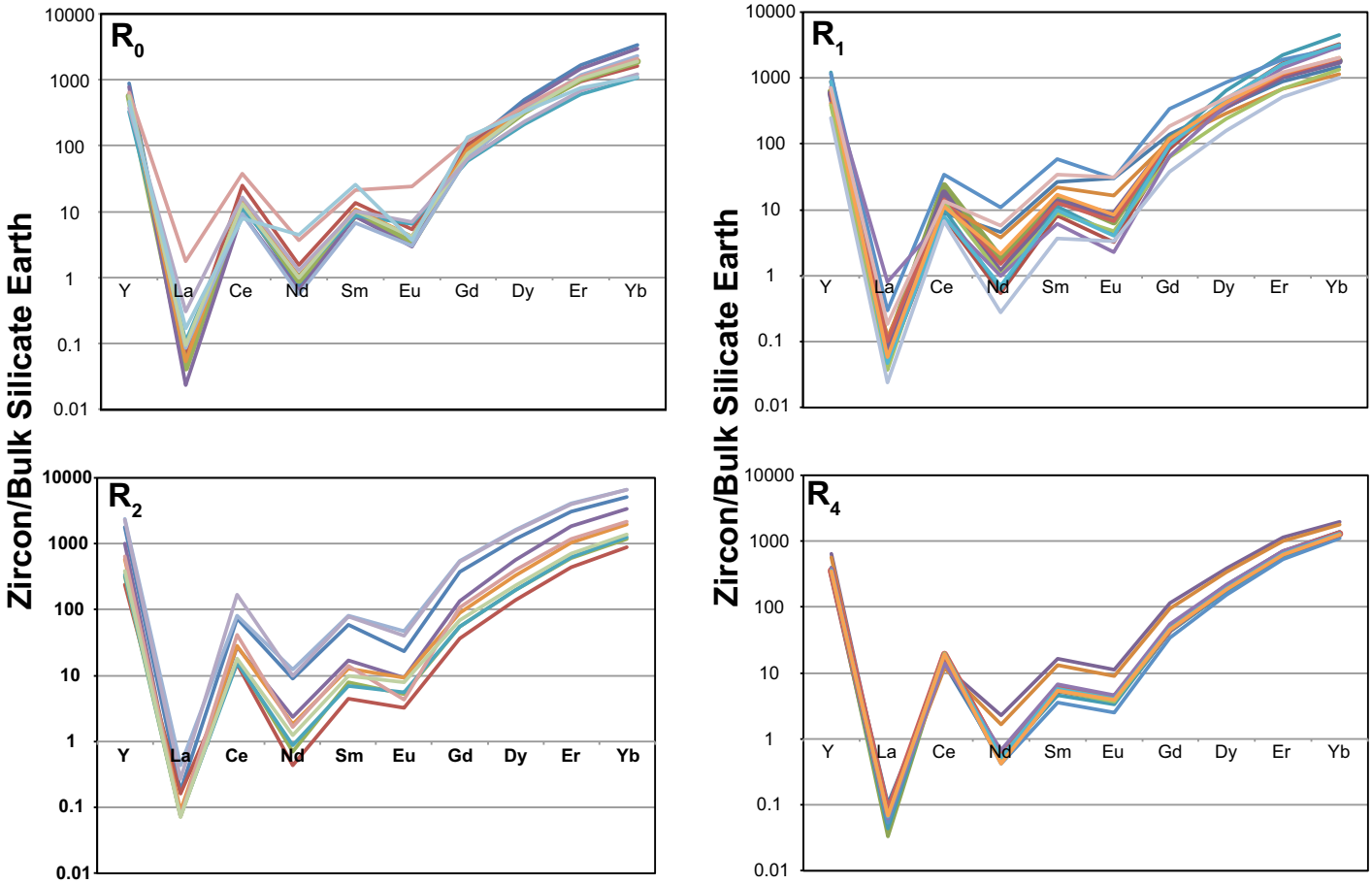

Figure 5. Rare earth element and Y diagrams for zircon from the Mineral King pendant rhyolites. Patterns within each sample showed a similar clustering of zircon compositions, with small populations that plot outside, typically with more enriched compositions. These few analyses that are more enriched than the bulk of the zircon population likely represent crystallization in a more evolved melt with the same system (as their age falls within the range of other zircon in each sample) or the analysis may have hit a small glass inclusion. However, the other parameters used to filter for inclusion did not suggest that the analysis was corrupted by an inclusion.

material in the upper crust across the history of the Mineral King units.

The uniformity of the zircon composition in the R_4 rhyolite suggests that the zircon grains it contains are not derived from diverse sources, such as preexisting crust or previous intrusions. Substantial incorporation of antecrystic zircon can produce wide variation in zircon trace element compositional populations (Klemetti et al., 2011). Combined with the high partition coefficient of most REEs into zircon, especially HREEs (Hanchar and van Westrenen, 2007), the tight clustering of the R_4 zircons across most trace element parameters (Figs. 6 and 7) would require a restricted magmatic source (compositionally and thermally) without much addition of crust or magma mixing. This could be produced by direct melting of the lower crust to produce the rhyolite or fractionation of the rhyolite from a basaltic parent, without significant interaction with the crustal column or a crustal column lacking in continental material of differing composition. In contrast, the diverse zircon compositional populations in the R_0, R_1, and R_2 rhyolites (Figs. 6 and 7) would be expected in a well-established magmatic system with abundant crystal recycling (Walker et al., 2010; Klemetti et al., 2011; Stelten and Cooper, 2012). The presence of xenocrystic zircon (1.63 Ga) in the R_0 rhyolite also supports the idea that continental crust had to have been incorporated into the batches of rhyolite magma.

These patterns in trace element compositions could be the product of fractional crystallization orassimilation of crustal material and/or precursory silicic intrusions (AFC). To determine which process plays the most significant role in the development of the trace element patterns for the Mineral King rhyolites, we constructed simple models of fractional crystallization of a rhyolite, using a low-Hf (high temperature) zircon from the R_1 unit (Table 2) as a starting composition and assimilation of crustal, silicic material into rhyolitic magmas (Fig. 10). Using partition coefficients (Supplemental Table 4[5]) for selected trace elements (U, Yb, Gd, Hf), an estimate of the trace element composition of the rhyolitic liquid in which the zircon crystallized was calculated (Table 2); this was used to model fractional crystallization using a modal assemblage of a typical unaltered rhyolite (55% quartz, 20% biotite, 20% plagioclase feldspar, 5% amphibole, 0.003% zircon) comparable to those found at the Mineral King pendant.

[5]Supplemental Table 4. Partition coefficients of minerals used in modeling fractional crystallization of rhyolite. Data sources for partition coefficients. Partition coefficients marked with asterisk are estimated based on little to no incorporation of element into mineral. Modal fraction for model based on visual estimates of the R_1 rhyolite. If you are viewing the PDF of this paper or reading it offline, please visit http://dx.doi.org/10.1130/GES00920.S5 or the full-text article on www.gsapubs.org to view Supplemental Table 4.

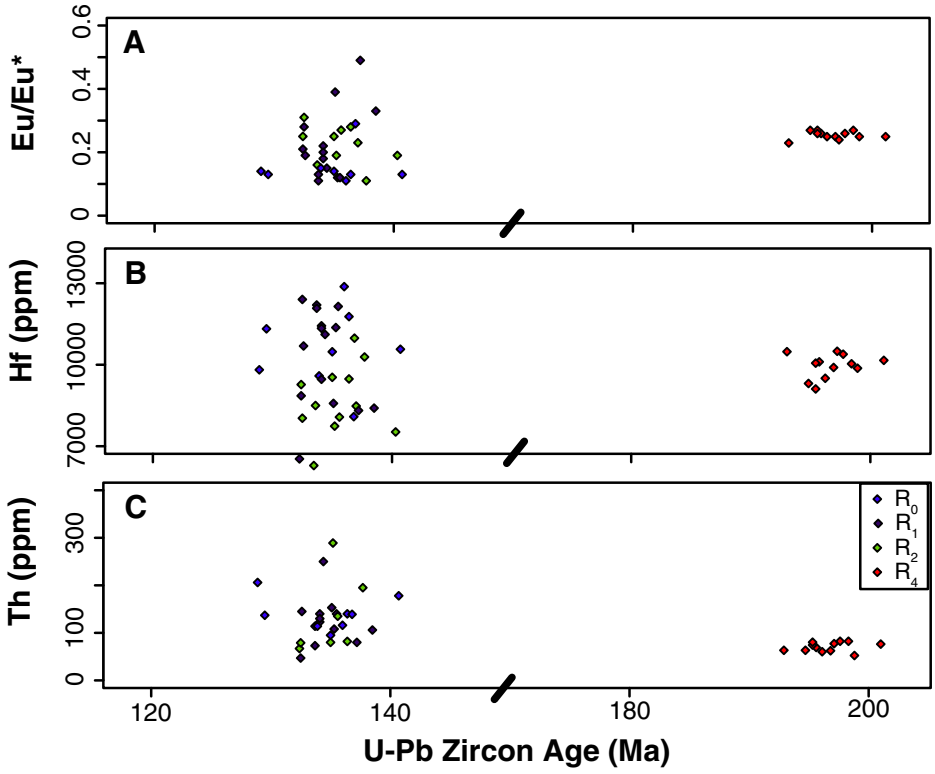

Figure 6. Zircon trace elements versus ^{207}Pb-corrected $^{206}Pb/^{238}U$ age for Mineral King rhyolites. Compositional changes of zircon over the Early Jurassic to Early Cretaceous. (A) Eu/Eu*. (B) Hf. (C) Th. The Early Jurassic rhyolite R_4 shows a much more restricted compositional range for all trace elements and ratios versus the Early Cretaceous rhyolites (R_0, R_1, and R_2).

Fractionation of this assemblage cannot account for the U/Yb diversity of zircon compositions found in the R_0, R_1, and R_2, because U/Yb is insensitive to fractionation (Fig. 10; Grimes et al., 2007). Instead, addition by assimilation of U-enriched continental crust (~5.4 ppm) by rhyolitic magma (Table 2; Fig. 10), likely accompanied by some fractional crystallization, best fits the pattern of increasing U/Yb with increasing Hf concentrations (Fig. 10). We chose to use a nearby granite that likely represents the composition of the middle to upper crust in the region (North Mountain; Wenner and Coleman, 2004). Although it is younger than the Mineral King rhyolites, these granites are voluminous and a good mix of melts extracted from the middle to upper crust, so they probably reflect the compositions of granitic melts (Table 2) that developed within the continental crust on the western margin of North American during the Jurassic to Cretaceous. The oldest R_4 (197 Ma) rhyolite required the least input of any crustal material, while the R_0, R_1, and R_2 (134–136 Ma) require the most input of crustal material to explain their compositional diversity (Fig. 10) in U/Yb versus Hf. The compositional spread of all zircons analyzed (Fig. 10; Supplemental Table 2 [see footnote 2]) can be explained by the wide range of partition coefficients for U, Yb, and Hf in zircon and potential small differences in parental rhyolite batches.

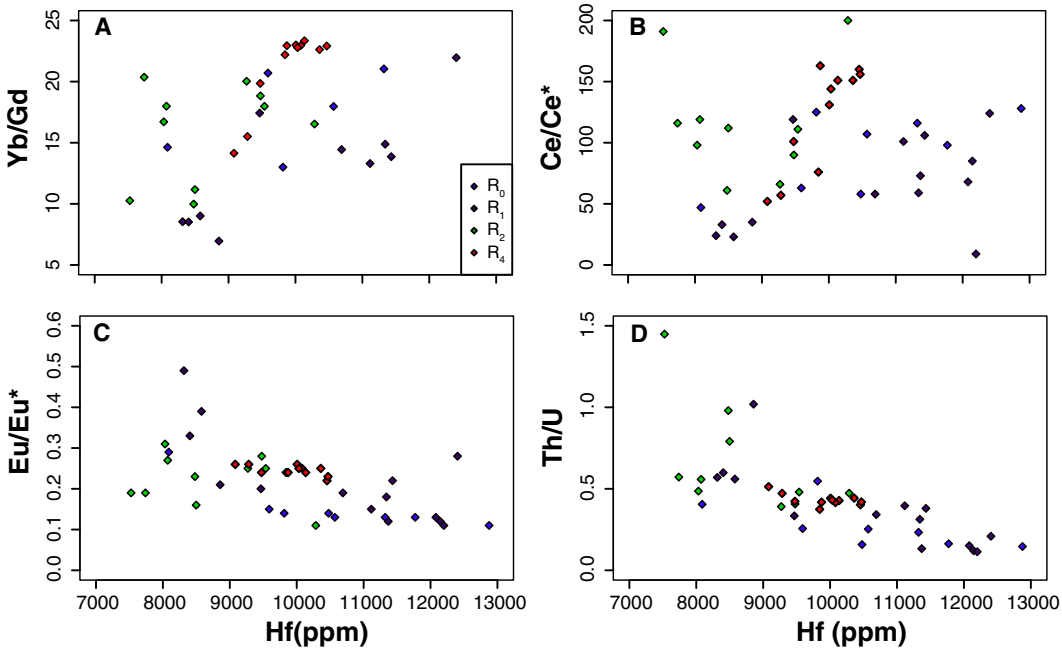

Figure 7. Trace elements versus Hf for Mineral King rhyolites. (A) Yb/Gd. (B) Ce/Ce*. (C) Eu/Eu*. (D) Th/U. In all four cases, the Early Jurassic rhyolite R_4 shows more clustering than the Early Cretaceous rhyolites (R_0, R_1, and R_2). However, all of the rhyolites plot within the same range of trace element compositions, suggesting a common origin later influenced by crustal involvement and crystal recycling.

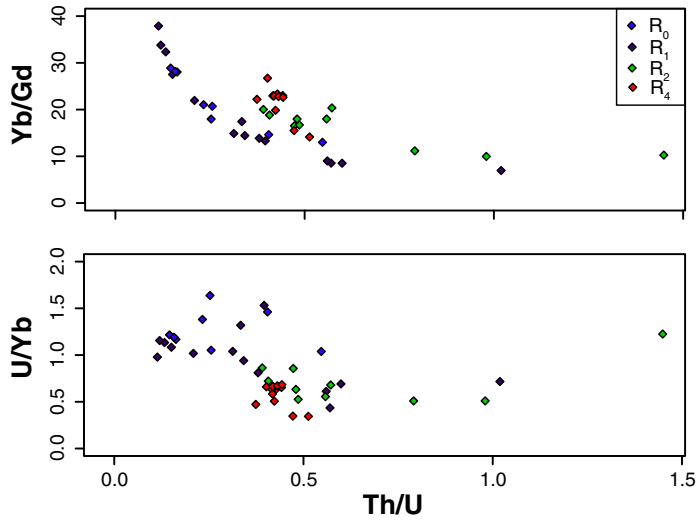

Figure 8. Yb/Gd and U/Yb versus Th/U for Mineral King rhyolites. Two trace element ratios from Barth et al. (2013) were used to assess the role of crust and fluids in the evolution of magmas. The top panel shows the variation in Yb/Gd, where the Early Jurassic rhyolite R_4 is tightly clustered relative to the Early Cretaceous rhyolites (R_0, R_1, and R_2). However, within the Early Cretaceous rhyolites, the R_2 has a distinct composition and the R_0 and R_1 overlap, suggesting that R_0 and R_1 may be the same unit. The lower panel shows variations in U/Yb indicating that neither suite of rhyolites was strongly influenced by slab fluids.

The $\delta^{18}O$(Zrn) values from the Mineral King rhyolites are considerably higher than the measured $\delta^{18}O$ (whole rock) values of 4.5‰–5.1‰ reported for two Mineral King metarhyolites (D'Errico et al., 2012). Thus, whole-rock $\delta^{18}O$ values of rhyolites in Mineral King have been lowered by exchange of these rocks by surface waters, possibly seawater or meteoric water. High-silica rhyolite and dacite metavolcanic rocks in the Sierra Nevada produced during high magmatic fluxes in the Mesozoic are in the range of 5.0‰–8.0‰ (Lackey et al., 2005, 2008). Thus, the Mineral King values are similar to values produced during high flux periods (Fig. 9C), rather than to values produced during magmatic lulls defined by Barth et al. (2013). Moreover, their $\delta^{18}O$ values do not indicate remelting of hydrothermally altered antecedent volcanic rocks, which would produce low $\delta^{18}O$ magma and possibly intracrystalline zoning such as seen at the Yellowstone caldera (Watts et al., 2012). Oxygen isotopic compositions are lowest [$\delta^{18}O$(Zrn) of ~5.3‰] in the R_4 rhyolite, suggesting that this rhyolite was derived from a more mantle-like parent (~5.3‰; Valley et al., 1998). Significant incorporation of continental crust or recycling of plutonic cumulates (mush) from the middle and upper crust that has not undergone significant hydrothermal alteration with low $\delta^{18}O$ (meteoric) waters should drive the $\delta^{18}O$(Zrn) in these magmas to higher values, as seen in the R_0 and R_1 rhyolites, where $\delta^{18}O$(Zrn) predicts magmatic values of ~8.7‰–9.3‰, higher than most known volcanic units of the same time period (Fig. 9C). These are $\delta^{18}O$ values similar to those observed in the modern central Andes of Chile, where highly thickened continental crust has a great influence on the compositions of the magmas erupted (James et al., 1985; Hildreth and Moorbath, 1988; Feeley and Sharp, 1995).

The Th compositions of zircons can also be sensitive to the presence of continental crustal or fractionated silicic material; the partition coefficient D_{Th} for zircon is not well constrained, but is likely high (estimates for peraluminous granite are as high as 22; Bea et al., 1994), so changes in the Th composition of crust being introduced into the magmatic system will be readily apparent. Magmas that have resided in and assimilated upper crustal material should have increased Th contents, as the upper crust has almost 10 times higher Th concentrations than the lower crust and ~1.6 times higher values than the middle crust (Rudnick and Gao, 2003). In addition, fractionating basaltic magmas should become enriched in Th, because it is highly incompatible (D < 0.01 in basalt; Weaver et al., 1986). Thus, any assimilation of previously existing crystal mushes will also increase Th concentrations of melt. The older R_4 rhyolites have relatively low Th contents, all <100 ppm (Fig. 6C). However, the younger R_0, R_1, and R_2 rhyolites have variable but higher Th contents, ranging into the hundreds to thousands of parts per million (Fig. 6C). This would support the incorporation of continental crust or silicic mushes into the magmas.

All of these lines of evidence (trace element models, oxygen isotopic compositions, Th content) suggest that the R_4 rhyolite, formed during the Early Jurassic, was minimally influenced by continental material or previously existing crystals mushes. This is different than the Triassic rhyolite in the Saddlebag Lake pendant studied by Barth et al. (2012), for which extraction from crystal mushes via rejuvenation is invoked for their formation. However, this is also in broad agreement with conclusions from Barth et al. (2013), where magmas produced during the Late Triassic–Early Jurassic magmatic lull show less evidence of crustal interactions. However, the Early Cretaceous R_0, R_1, and R_2 rhyolites reflect extraction from a preexisting crystal mush with contributions from continental crust.

Ramifications for Pre–Sierra Nevada Batholith Magmatism

The rhyolites of the Mineral King pendant provide a window into two periods of caldera volcanism along the western margin of North America; they also record information from periods considered as "background level" of magmatic production compared to episodes of voluminous magmatism in the Middle Jurassic and middle to Late Cretaceous (Irwin and Wooden, 2001; Barth et al., 2013; Fig. 10). Therefore, they also provide useful insight into the sources of magmas during these quiescent periods. Recent discussion of changing zircon trace element chemistry in the detrital record suggests that magmatic lulls record different magma compositions that may be linked to lower budgets of slab-derived fluid and minimal crustal involvement, possibly as a result of large-scale extension or transtension in the arc (Barth et al., 2013). Comparison of the Mineral King data to those key ratios of U/Yb, Th/U, and Yb/Gd used by Barth et al. (2013) shows that the Mineral King rhyolite magmas are broadly similar in composition to magmas sampled in the detrital zircon record for the two lulls identified by Barth et al. (2013) in the Late Triassic–Early Jurassic (lull 1) and Late Jurassic–Early Cretaceous (lull 2). However, there are some key differences from the conclusions of Barth et al. (2013). The R_4 rhyolite, which was within lull 1, has much lower Yb/Gd, suggesting that zircon grew from a more HREE-depleted melt

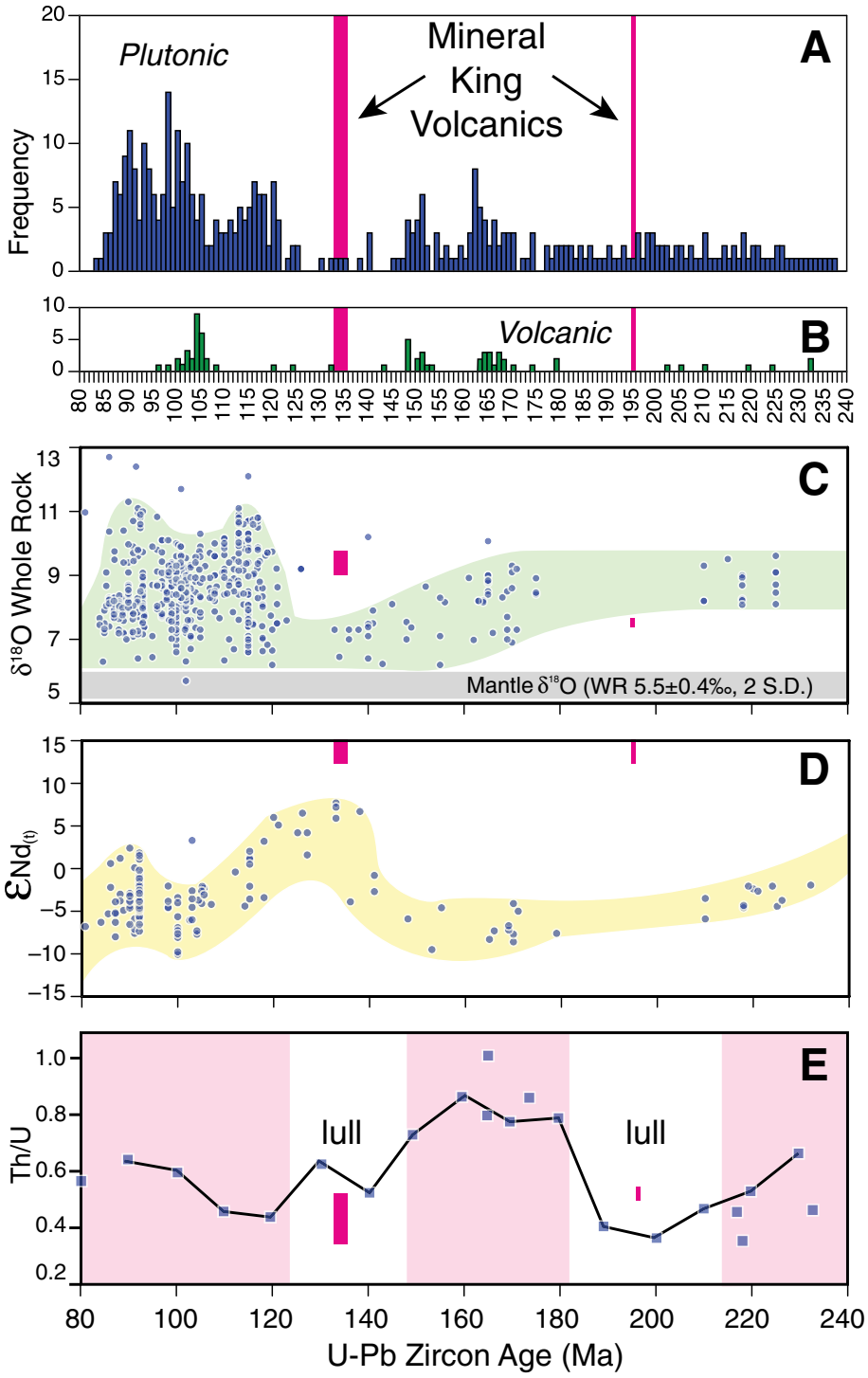

Figure 9. Age, $\delta^{18}O$, εNd, and Th/U for zircon across the Sierra Nevada. Pink bars indicate magmatic lulls. (A, B) Overall U-Pb zircon age distribution of igneous zircon from the Sierra Nevada. The Mineral King samples are in red vertical bars, showing their locations with respect to prominent lulls. (C) Variation in $\delta^{18}O$ for Sierra Nevada zircon. Mineral King zircons are lower than most Sierra Nevada zircons, but still show strong evidence for crustal contamination. WR—whole rock; S.D.—standard deviation. (D) εNd for zircon, showing an increase during the two magmatic lulls. Values extrapolated from trends across data set. (E) Th/U for zircon across the Sierra Nevada. Data sources used to lay out figure are described in the Supplemental File (which can be viewed by visiting http://dx.doi.org/10.1130/GES00920.S6 or the full-text article on www.gsapubs.org).

than other lull 1 magmas or at higher crystallization temperatures (Figs. 8 and 11). The R_0, R_1, and R_2 rhyolites have much lower Th/U than other lull 2 magmas (Fig. 9E), while Yb/Gd and U/Yb span larger ranges (Figs. 8 and 11). These observations suggest that the R_0, R_1, and R_2 rhyolite magmas were influenced little by slab fluids. These rhyolites also have a higher whole-rock $\delta^{18}O$ [based on $\delta^{18}O$(Zrn)] than the few other volcanic units sampled within lull 2 (Fig. 9C).

Barth et al. (2013) implied that magma produced during the magmatic lulls had minimal crustal involvement. However, the $\delta^{18}O$(Zrn) values of the 134–136 Ma rhyolites (Table 1) clearly show a stronger influence of crustal material in their evolution, as do the trace element models (Fig. 10) and Th concentrations (Fig. 6C) found in zircon. The production of rhyolite with $\delta^{18}O$(Zrn) values of 5.3‰ at 195 Ma (R_4) is consistent with partial melting of lower crust and little involvement of crustal melts; however, the later (134–136 Ma) rhyolites (R_0, R_1, and R_2) in the pendant show higher crustal inputs, albeit not at levels shown for some >10‰ granites in the Cretaceous (Lackey et al., 2008; Fig. 9). Therefore, the notion of magmatic lulls being background magma production periods with less crustal influence does not appear to be supported by the Early Cretaceous rhyolites at the Mineral King pendant. However, relative to the peak magmatism in the Sierra Nevada from the Triassic to the Cretaceous, the 134–136 Ma rhyolites of the Mineral King pendant do not show contamination that is as extensive, likely reflecting the lower rates of magma supply into the arc during these lulls.

The Early Jurassic magmatism (R_4) has much less evidence for the influence of continental crust or magmatic precursors, but by the Early Cretaceous (R_0, R_1, and R_2), it is clear that continental crust and magmatic recycling played a much larger role in magma genesis. This mirrors the tectonic evolution of western North America, where the continued accretion of exotic terranes to the continent caused a change in the nature of the crust (Schweickert and Lahren, 1993; Ernst, 2010; Barth et al., 2012; Holland et al., 2013). Arc magmatism off North America was probably in the form of island arcs that docked with North America during the Jurassic (Irwin and Wooden, 1999, 2001). The R_4 rhyolite is likely the product of one of these more primitive arcs, as the rhyolite shows little influence of continental crust in oxygen or trace element compositions. This might be similar to rhyolite magmas erupted in island arcs such as the modern Kermadec Islands (Graham et al., 2008) or Mariana Islands (Reagan et al., 2008).

TABLE 2. PARAMETERS FOR FRACTIONAL CRYSTALLIZATION AND ASSIMILATION MODELS

	U (ppm)	Yb (ppm)	Gd (ppm)	Hf (ppm)
R_1 zircon (11MK02-2.1)	140	322	38	8314
Calculated rhyolite from R_1 zircon	0.55	1.16	4.75	2.77
Crust composition for assimilation model	5.4	1.84	1.96	4.18

Note: See Supplemental Table 4 (see text footnote 5) for partition coefficients used to calculate the rhyolite composition from the R_1 zircon analysis. Crust composition is from Wenner and Coleman (2004), sample NM98-1.

However, as the accretion of arc material progressed into the Early Cretaceous, the influence of continental crust was greater. The $\delta^{18}O$ of rhyolite erupted during the Early Cretaceous is much higher than that of the Early Jurassic (Fig. 11C); this is typically interpreted as a signal of continental crust influence (Lackey et al., 2008; Barth et al., 2013). The wider range of trace element compositions in the R_0, R_1, and R_2 rhyolite zircons also reflect an increased component of crustal recycling, as zircons from different pockets of subvolcanic crystallizing magma capture the variations in magma composition as new magmas intrude (Claiborne et al., 2010a; Klemetti et al., 2011) and smaller batches of magma fractionate (Storm et al., 2011). These crystals are subsequently sampled during each eruption of the volcano associated with each eruptive package (Claiborne et al., 2010b; Klemetti et al., 2011; Stelten and Cooper, 2012). This change reflects the thickening of the crust leading toward the intrusion of the Sierra Nevada batholith. It may be this priming of the crust during the millions of years before the large pulse of granitic magmas that allows for such voluminous magmatism in the crust (e.g., Lipman, 2007; Grunder et al., 2008; Walker et al., 2010). Even though these Early Cretaceous rhyolites of the Mineral King pendant may be scarce in the modern surface rock record across the Sierra Nevada province, the eruption of voluminous rhyolites that show the evidence of long-lived magmatism may be one of the key events that allowed for the intrusion of the batholith in the Late Cretaceous.

CONCLUSIONS

The rhyolite tuffs and flows found in the Mineral King pendant, dated using U-Pb spot ages of zircon, represent a combination of allochthonous Late Triassic (195.7 ± 1.4 Ma) and Early Cretaceous volcanic deposits (134.2–136.5 Ma). The distribution of ages from the Mineral King pendant suggests a complex origin. The original chronology for the units in the septum from Busby-Spera (1983) had the rhyolite units becoming younger to the west as a continuous depositional sequence and all units being Triassic in age. However, the new zircon ages presented here show that only one unit is Triassic in age and the rest are Early Cretaceous, suggesting that the pendant most likely was brought together through structural means after the emplacement (134.2 Ma) of the youngest rhyolite.

The 196 Ma and 134–136 Ma rhyolite units represent one of the few records of magmatism for two periods recognized as lulls in magmatic activity across the Late Triassic to Early Cretaceous in western North American margin. The evidence from zircon ages and compositions suggests that magma from the Sierra Nevada arc during the Early Cretaceous was interacting with North American crust, with increasing crustal influence from the Early Jurassic to Early Cretaceous, following the evolution of the western margin of the continent from an island to continental arc. This evidence includes xenocrystic zircon with ages older than 1.6 Ga, $\delta^{18}O$(Zrn) compositions of zircons from the 134–136 Ma rhyolite that are ~6.7‰–7.3‰ (rhyolite composition of ~8.7‰–9.3‰), and trace element compositions that are consistent with a highly fractionated composition similar to granite of the Late Cretaceous Sierran Arc. There is also strong evidence in U/Yb and Th compositions of zircon that requires the input of continental crust into the 134–136 Ma rhyolite units relative to the 197 Ma rhyolite within the Mineral King pendant. This evidence of Early Cretaceous magmatism shows that even though the record of volcanism is scant within the Sierra Nevada arc, voluminous caldera magmatism was occurring along the western margin of North America as continental crust developed.

These data also show how examination of spot ages and trace element analyses of zircon combined with bulk zircon oxygen isotopic data can help unravel the petrogenesis of altered volcanic

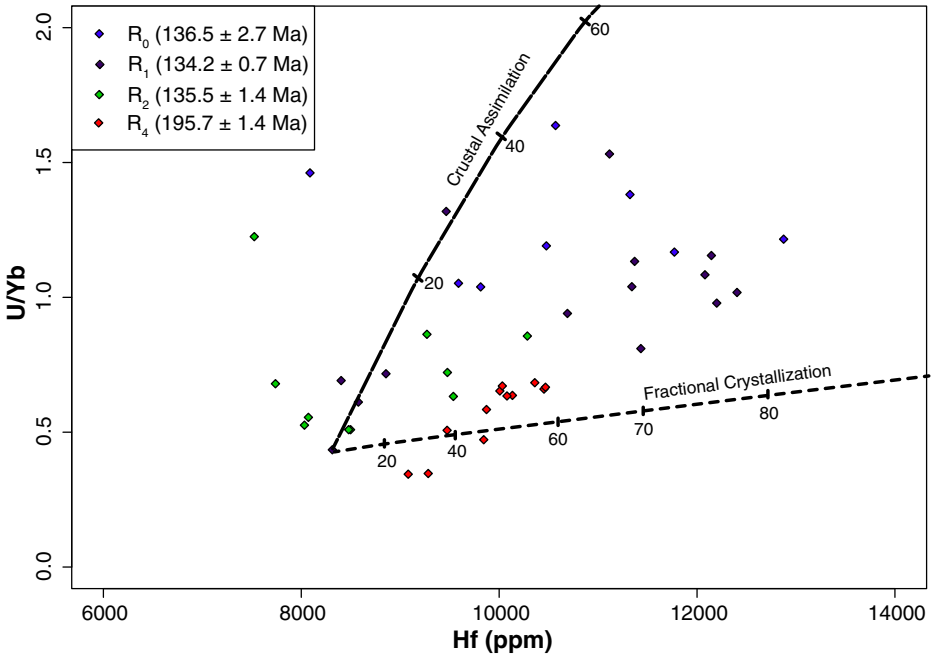

Figure 10. Fractional crystallization and assimilation models for the potential compositional variation of zircon in Mineral King pendant rhyolites. U/Yb versus Hf is plotted; models are of fractional crystallization of a rhyolite assemblage (see text) and assimilation of upper-middle crustal silicic intrusions from the area around the Mineral King pendant (based on the granite of North Mountain; Wenner and Coleman, 2004). The R_4 (Early Jurassic, lull 1 in Barth et al., 2013) rhyolite requires little addition of crustal material to account for the U/Yb vs. Hf of the zircon, supporting the oxygen isotopic and Th evidence that evolved continental crust played a negligible role in its genesis. The R_0, R_1, and R_2 rhyolites (Early Cretaceous, lull 2 in Barth et al., 2013) require the addition of silicic material with elevated U to produce the elevated U/Yb versus Hf in all rhyolite unit zircons. This addition of crustal material is supported by the higher $\delta^{18}O$(Zrn) and elevated Th seen in zircon from the R_0, R_1, and R_2 rhyolites.

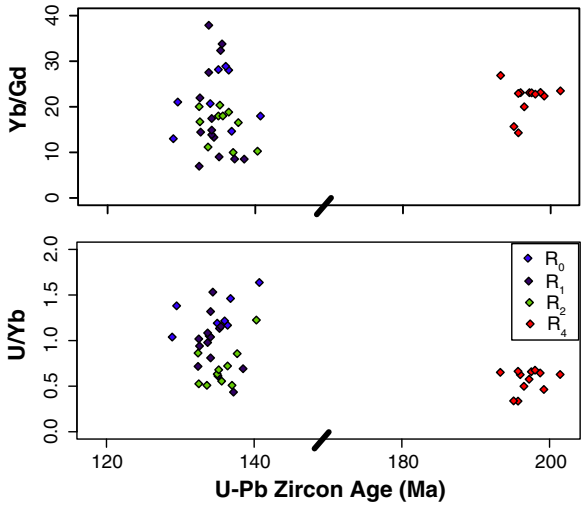

Figure 11. Yb/Gd and U/Yb versus ^{207}Pb-corrected $^{206}Pb/^{238}U$ age. The top panel shows changes in Yb/Gd. The lower panel is U/Yb versus age, showing the changes in composition from the Early Jurassic (R_4) to the Early Cretaceous (R_0, R_1, and R_2) rhyolites. Note the difference in overall composition of the R_2 and R_0 and R_1 rhyolites, suggesting that the R_0 and R_1 are the same unit.

rocks. The signatures of fractional crystallization and assimilation are recorded in the trace element composition of zircon, and the resistance of zircon to alteration (unlike whole-rock or major phases) allows for the estimation of the relative importance of these processes in the formation of volcanic units. Improved constraints on the partitioning of trace elements into zircon at different compositions and conditions will permit further exploitation of these methods to explain the petrogenesis of ancient volcanic rocks.

ACKNOWLEDGMENTS

We thank David Greene, Megan D'Errico, and Staci Loewy for assistance during field work (summer 2010, 2011) and Joe Wooden and Matt Coble (Stanford University) for assistance with the SHRIMP-RG (sensitive high-resolution ion microprobe–reverse geometry) analyses. We also thank Ilya Bindeman (University of Oregon) for assistance with the oxygen isotope analyses and the National Park Service for permitting sampling for this project. Funding for this research was provided by the Keck Geology Consortium and the Denison University Undergraduate Research Fund. The Pomona College XRF Laboratory is partly supported by National Science Foundation Division of Undergraduate Education grant CCLI 0942447 and Pomona College. Partical support comes from NSF grant EAR-0948706 to Lackey. We also thank Jamey Jones, Craig Grimes, and a third anonymous reviewer for their comments on earlier versions of this manuscript.

REFERENCES CITED

Barth, A.P., Feilen, A.D.G., Yager, S.L., Douglas, S.R., Wooden, J.L., Riggs, N.R., and Walker, J.D., 2012, Petrogenetic connections between ash-flow tuffs and a granodioritic to granitic intrusive suite in the Sierra Nevada arc, California: Geosphere, v. 8, p. 250–264, doi:10.1130/GES00737.1.

Barth, A.P., Wooden, J.L., Jacobsen, C.E., and Economos, R.C., 2013, Detrital zircon as a proxy for tracking the magmatic arc system: The California arc example: Geology, v. 41, doi:10.1130/G33619.1.

Bateman, P.C., 1992, Plutonism in the central part of the Sierra Nevada Batholith, California: U.S. Geological Survey Professional Paper 1483, 186 p.

Bea, F., Pereira, M.D., and Stroh, A., 1994, Mineral/leucosome trace-element partitioning in a peraluminous migmatite (a laser ablation-ICP-MS study): Chemical Geology, v. 117, p. 291–312, doi:10.1016/0009-2541(94)90133-3.

Bindeman, I.N., 2008, Oxygen isotopes in mantle and crustal magmas as revealed by single crystal analysis: Reviews in Mineralogy and Geochemistry, v. 69, p. 445–478, doi:10.2138/rmg.2008.69.12.

Busby-Spera, C.J., 1983, Paleogeographic reconstruction of a submarine volcanic center: Geochronology of the Mineral King roof pendant, Sierra Nevada, California [Ph.D. thesis]: Princeton, New Jersey, Princeton University, 190 p.

Busby-Spera, C.J., 1984, Large-volume rhyolite ash flow eruptions and submarine caldera collapse in the Lower Mesozoic Sierra Nevada, California: Journal of Geophysical Research, v. 89, no. B10, p. 8417–8427, doi:10.1029/JB089iB10p08417.

Busby-Spera, C.J., 1986, Depositional features of rhyolitic and andesitic volcaniclastic rocks of the Mineral King submarine caldera complex, Sierra Nevada, California: Journal of Volcanology and Geothermal Research, v. 27, p. 43–76, doi:10.1016/0377-0273(86)90080-6.

Busby-Spera, C.J., and Saleeby, J., 1987, Geologic guide to the Mineral King area, Sequoia National Park, California: Pacific Section, Society of Economic Paleontologists and Mineralogists Guidebook 56, 44 p.

Chen, J.H., and Moore, J.G., 1982, Uranium-lead isotopic ages from the Sierra Nevada Batholith, California: Journal of Geophysical Research, v. 87, no. B6, 4761, doi:10.1029/JB087iB06p04761.

Claiborne, L.L., Miller, C.F., and Wooden, J.L., 2010a, Trace element composition of igneous zircon: a thermal and compositional record of the accumulation and evolution of a large silicic batholith, Spirit Mountain, Nevada: Contributions to Mineralogy and Petrology, v. 160, p. 511–531, doi:10.1007/s00410-010-0491-5.

Claiborne, L.L., Miller, C.F., Flanagan, D.M., Clynne, M.A., and Wooden, J.L., 2010b, Zircon reveals protracted magma storage and recycling beneath Mount St. Helens: Geology, v. 38, p. 1011–1014, doi:10.1130/G31285.1.

DeCelles, P.G., Ducea, M., Kapp, P., and Zandt, G., 2009, Cyclicity in Cordilleran orogenic systems: Nature Geoscience, v. 2, p. 251–257, doi:10.1038/ngeo469.

D'Errico, M.E., Lackey, J.S., Surpless, B.E., Loewy, S.L., Wooden, J.L., Barnes, J.D., Strickland, A., and Valley, J.W., 2012, A detailed record of shallow hydrothermal fluid flow in the Sierra Nevada magmatic arc from low-^{18}O skarn garnets: Geology, v. 40, p. 763–766, doi:10.1130/G33008.1.

Dietterich, H.R., Lackey, J.S., and Bindeman, I., 2009, Origin and alteration of Triassic metavolcanic rocks in the Saddlebag Lake Pendant, eastern Sierra Nevada: Geological Society of America, https://gsa.confex.com/gsa/2009CD/finalprogram/abstract_157536.htm.

Ernst, W.G., 2010, Young convergent-margin orogens, climate and crustal thickness—A Late Cretaceous–Paleogene Nevadoplano in the American Southwest?: Lithosphere, v. 2, p. 67–75, doi:10.1130/L84.1.

Feeley, T.C., and Sharp, Z.D., 1995, $^{18}O/^{16}O$ isotope geochemistry of silicic lava flows erupted from Volcán Ollagüe, Andean Central Volcanic Zone: Earth and Planetary Science Letters, v. 133, p. 239–254, doi:10.1016/0012-821X(95)00094-S.

Fiske, R.S., and Tobisch, O.T., 1994, Middle Cretaceous ash-flow tuff and caldera-collapse deposit in the Minarets Caldera, east-central Sierra Nevada, California: Geological Society of America Bulletin, v. 106, p. 582, doi:10.1130/0016-7606(1994)106<0582:MCAFTA>2.3.CO;2.

Glazner, A.F., Bartley, J.M., Coleman, D.S., Gray, W., and Taylor, R.Z., 2004, Are plutons assembled over millions of years by amalgamation from small magma chambers?: GSA Today, v. 14, no. 4/5, p. 4–11, doi:10.1130/1052-5173(2004)014<0004:APAOMO>2.0.CO;2.

Graham, I.J., Reyes, A.G., Wright, I.C., Peckett, K.M., Smith, I.E.M., and Arculus, R.J., 2008, Structure and petrology of newly discovered volcanic centers in the northern Kermadec–southern Tofua arc, South Pacific Ocean: Journal of Geophysical Research, v. 113, no. B8, doi:10.1029/2007JB005453.

Grimes, C.B., John, B.E., Kelemen, P.B., Mazdab, F.K., Wooden, J.L., Cheadle, M.J., Hanghøj, K., and Schwartz, J.J., 2007, Trace element chemistry of zircons from oceanic crust: A method for distinguishing detrital zircon provenance: Geology, v. 35, p. 643–646, doi:10.1130/G23603A.1.

Grunder, A.L., Klemetti, E.W., Feeley, T.C., and McKee, C.M., 2008, Eleven million years of arc volcanism at the Aucanquilcha Volcanic Cluster, northern Chilean Andes: Implications for the life span and emplacement of plutons: Royal Society of Edinburgh Transactions, Earth Sciences, v. 97, p. 415–436, doi:10.1017/S0263593300001541.

Hanchar, J.M., and van Westrenen, W., 2007, Rare earth element behavior in zircon-melt systems: Elements, v. 3, p. 37–42, doi:10.2113/gselements.3.1.37.

Hanson, R.B., Sorensen, S.S., Barton, M.D., and Fiske, R.S., 1993, Long-term evolution of fluid-rock interactions in magmatic arcs: Evidence from the Ritter Range pendant, Sierra Nevada, California, and numerical modeling: Journal of Petrology, v. 34, p. 23–62, doi:10.1093/petrology/34.1.23.

Harley, S.L., and Kelly, N.M., 2007, Zircon, tiny but timely: Elements, v. 3, p. 13–18, doi:10.2113/gselements.3.1.13.

Hildreth, W., and Moorbath, S., 1988, Crustal contributions to arc magmatism in the Andes of central Chile: Contributions to Mineralogy and Petrology, v. 98, p. 455–489, doi:10.1007/BF00372365.

Holland, J.E., Surpless, B.E., Smith, D.R., Loewy, S.L., and Lackey, J.S., 2013, Intrusive history and petrogenesis of the Ash Mountain Complex, Sierra Nevada batholith, California (USA): Geosphere, v. 9, p. 691–717, doi:10.1130/GES00890.1.

Irwin, W.P., and Wooden, J.L., 1999, Plutons and accretionary episodes of the Klamath Mountains, California and Oregon: U.S. Geological Survey Open-File Report 99-374, 1 p.

Irwin, W.P., and Wooden, J.L., 2001, Map showing plutons and accreted terranes of the Sierra Nevada, California with a tabulation of U/Pb isotopic ages: U.S. Geological Survey Open-File Report 2001-229, scale 1:100,000.

James, D.E., Harmon, R.S., and Barreiro, B.A., 1984, Quantitative models for crustal contamination in the central and northern Andes, *in* Harmon, R.S., and Barreiro, B.A., eds., Andean magmatism: Chemical and isotopic constraints: Nantwich, UK, Shiva Publishers, p. 124–138, 231–250.

King, E.M., Barrie, C.T., and Valley, J.W., 1997, Hydrothermal alteration of oxygen isotope ratios in quartz phenocrysts, Kidd Creek Mine, Ontario: Magmatic values are preserved in zircon: Geology, v. 25, p. 1079–1082, doi:10.1130/0091-7613(1997)025<1079:HAOOIR>2.3.CO;2.

Kistler, R.W., and Swanson, S.E., 1981, Petrology and geochronology of metamorphosed volcanic rocks

and a middle Cretaceous volcanic neck in the east-central Sierra Nevada, California: Journal of Geophysical Research, v. 86, no. B11, 10489, doi:10.1029/JB086iB11p10489.

Klemetti, E.W., Deering, C.D., Cooper, K.M., and Roeske, S.M., 2011, Magmatic perturbations in the Okataina Volcanic Complex, New Zealand at thousand-year timescales recorded in single zircon crystals: Earth and Planetary Science Letters, v. 305, p. 185–194, doi:10.1016/j.epsl.2011.02.054.

Lackey, J.S., Valley, J.W., and Saleeby, J.B., 2005, Supracrustal input to magmas in the deep crust of Sierra Nevada batholith: evidence from high-$\delta^{18}O$ zircon: Earth and Planetary Science Letters, v. 235, p. 315–330, doi:10.1016/j.epsl.2005.04.003.

Lackey, J.S., Valley, J.W., Chen, J.H., and Stockli, D.F., 2008, Evolving magma systems, crustal recycling, and alteration in the central Sierra Nevada batholith: The oxygen isotope record: Journal of Petrology, v. 49, p. 1397–1426, doi:10.1093/petrology/egn030.

Lackey, J.S., Cecil, M.R., Windham, C.J., Frazer, R.E., Bindeman, I.N., and Gehrels, G., 2012, The Fine Gold Intrusive Suite: The roles of basement terranes and magma source development in the Early Cretaceous Sierra Nevada batholith: Geosphere, v. 8, p. 292–313, doi:10.1130/GES00745.1.

Lackey, J.S., Cecil, M.R., Miller, J.S., Sendek, C.L., Eisenberg, J.L., Economos, R., and Davies, G.R., 2013, Small volume peraluminous granites as windows into anatectic conversion of accreted terranes to crust in continental arcs: Geological Society of America Abstracts with Programs, v. 45, no. 6, p. 56.

Lipman, P.W., 2007, Incremental assembly and prolonged consolidation of Cordilleran magma chambers: Evidence from the Southern Rocky Mountain volcanic field: Geosphere, v. 3, p. 42–70, doi:10.1130/GES00061.1.

Ludwig, K.R., 2003, User's manual for Isoplot 3.00: A geochronological toolkit for Microsoft Excel: Berkeley, California, Berkeley Geochronology Center Special Publication 4, 74 p.

Mazdab, F.K., and Wooden, J.L., 2006, Trace element analysis in zircon by ion microprobe (SHRIMP-RG): Technique and applications: Geochimica et Cosmochimica Acta, v. 70, p. A405, doi:10.1016/j.gca.2006.06.817.

Miller, C.F., McDowell, S.M., and Mapes, R.W., 2003, Hot or cold granites? Implications of zircon saturation temperatures and preservation of inheritance: Geology, v. 31, no. 6, p. 529–532.

Paterson, S., 2012, Tectonic and magmatic tempos in the Mesozoic central Sierra Nevada arc: Geological Society of America Abstracts with Programs, v. 44, no. 7, p. 489.

Reagan, M.K., Hanan, B.B., Heizler, M.T., Hartman, B.S., and Hickey-Vargas, R., 2008, Petrogenesis of volcanic rocks from Saipan and Rota, Mariana Islands, and implications for the evolution of nascent island arcs: Journal of Petrology, v. 49, p. 441–464, doi:10.1093/petrology/egm087.

Rudnick, R.L., and Gao, S., 2003, Composition of the continental crust, *in* Rudnick, R.L., ed., Treatise on Geochemistry 3: New York, Elsevier, p. 1–64, doi:10.1016/B0-08-043751-6/03016-4.

Saleeby, J.B., and Busby, C., 1993, Paleogeographic and tectonic setting of axial and western metamorphic framework rocks of the southern Sierra Nevada, California, *in* Dunne, G.C., and McDougall, K., eds., Mesozoic paleogeography of the Western United States-II: Pacific Section, Society of Economic Paleontologists and Mineralogists Book 71, p. 197–225.

Saleeby, J., Goodin, S., Sharp, W.D., and Busby, C., 1978, Early Mesozoic paleotectonic-paleogeographic reconstruction of the southern Sierra Nevada region, *in* Howell, G., and McDougall, G., eds., Mesozoic paleogeography of the western United States: Pacific Coast Paleogeography Symposium 2: Los Angeles, Society of Economic Paleontologists and Mineralogists, p. 311–336.

Saleeby, J.B., Kistler, R.W., Longiaru, S.J., Moore, J.G., and Nokleberg, W.J., 1990, Middle Cretaceous silicic metavolcanic rocks in the Kings Canyon area, central Sierra Nevada, California, *in* Anderson, L., ed., The nature and origin of Cordilleran magmatism: Geological Society of America Memoir 174, p. 251–270, doi:10.1130/MEM174-p251.

Sano, Y., Terada, K., and Fukuoka, T., 2002, High mass resolution ion microprobe analysis of rare earth elements in silicate glass, apatite and zircon: Lack of matric dependency: Chemical Geology, v. 184, p. 217–230, doi:10.1016/S0009-2541(01)00366-7.

Schweickert, R.A., and Lahren, M.M., 1993, Triassic–Jurassic magmatic arc in eastern California and western Nevada: Arc evolution, cryptic tectonic breaks and significance of the Mojave–Snow Lake fault, *in* Dunn, G., and McDougall, K., eds., Mesozoic paleogeography of the Western United States-II: Pacific Section, Society of Economic Paleontologists and Mineralogists Book 71, p. 227–246.

Schweickert, R.A., and Lahren, M.M., 1999, Triassic caldera at Tioga Pass, Yosemite National Park, California: Structural relationships and significance: Geological Society of America Bulletin, v. 111, p. 1714–1722, doi:10.1130/0016-7606(1999)111<1714:TCATPY>2.3.CO;2.

Sisson, T.W., and Moore, J.G., 2013, Geologic map of southwestern Sequoia National Park, Tulare County, California: U.S. Geological Survey Open-File Report 2013–1096, 26 p., 2 sheets, scale 1:24,000.

Sorensen, S.S., Dunne, G.C., Hanson, R.B., Barton, M.D., Becker, J., Tobisch, O.T., and Fiske, R.S., 1998, From Jurassic shores to Cretaceous plutons: Geochemical evidence for paleoalteration environments of metavolcanic rocks, eastern California: Geological Society of America Bulletin, v. 110, p. 326–343, doi:10.1130/0016-7606(1998)110<0326:FJSTCP>2.3.CO;2.

Stelten, M.E., and Cooper, K.M., 2012, Constraints on the nature of the subvolcanic reservoir at South Sister volcano, Oregon from U-series dating combined with subcrystal trace-element analysis of plagioclase and zircon: Earth and Planetary Science Letters, v. 313–314, p. 1–11, doi:10.1016/j.epsl.2011.10.035.

Storm, S., Shane, P.A., Schmitt, A.K., and Lindsay, J.M., 2011, Contrasting punctuated zircon growth in two syn-erupted rhyolite magmas from Tarawera volcano: Insights into crystal diversity in magmatic systems: Earth and Planetary Science Letters, v. 301, p. 511–520, doi:10.1016/j.epsl.2010.11.034.

Valley, J.W., Kitchen, N., Kohn, M.J., Niendorf, C.R., and Spicuzza, M.J., 1995, UWG-2, a garnet standard for oxygen isotope ratios: Strategies for high precision and accuracy with laser heating: Geochimica et Cosmochimica Acta, v. 59, p. 5223–5231, doi:10.1016/0016-7037(95)00386-X.

Valley, J.W., Kinny, P.D., Schulze, D.J., and Spicuzza, M.J., 1998, Zircon megacrysts from kimberlite: Oxygen isotope variability among mantle melts: Contributions to Mineralogy and Petrology, v. 133, p. 1–11, doi:10.1007/s004100050432.

Walker, B.A., Jr., Grunder, A.L., and Wooden, J.L., 2010, Organization and thermal maturation of long-lived arc systems: Evidence from zircons at the Aucanquilcha volcanic cluster, northern Chile: Geology, v. 38, p. 1007–1010, doi:10.1130/G31226.1.

Watts, K.E., Bindeman, I.N., and Schmitt, A.K., 2012, Crystal scale anatomy of a dying supervolcano: An isotope and geochronology study of individual phenocrysts from voluminous rhyolites of the Yellowstone caldera: Contributions to Mineralogy and Petrology, v. 164, p. 45–67, doi:10.1007/s00410-012-0724-x.

Weaver, B.L., Wood, D.A., Tarney, J., and Joron, J.L., 1986, Role of subducted sediment in the genesis of ocean-island basalts: Geochemical evidence from South Atlantic Ocean islands: Geology, v. 14, p. 275, doi:10.1130/0091-7613(1986)14<275:ROSSIT>2.0.CO;2.

Wenner, J.M., and Coleman, D.S., 2004, Magma mixing and Cretaceous crustal growth: Geology and geochemistry of granites in the Central Sierra Nevada Batholith, California: International Geology Review, v. 46, p. 880–903, doi:10.2747/0020-6814.46.10.880.